Supplementary Material: Light induced Exciton Spin Hall Effect in Van der Waals Heterostructures

Yun-Mei Li,[1] Jian Li,[1] Li-Kun Shi,[2] Dong Zhang,[1] Wen Yang,[2] and Kai Chang[1,3,*]

[1]*SKLSM, Institute of Semiconductors, Chinese Academy of Sciences, P.O. Box 912, Beijing 100083, China*
[2]*Beijing Computational Science Research Center, Beijing 100094, China*
[3]*Synergetic Innovation Center of Quantum Information and Quantum Physics, University of Science and Technology of China, Hefei, Anhui 230026, China*

S1. FIRST-PRINCIPLES CALCULATIONS OF THE WSE_2/$MOSE_2$ VAN DER WAALS HETEROSTRUCTURES

We apply the density functional theory (DFT)[1] performed by the Vienna ab initio Simulation Package (VASP)[2] with the projector augmented wave (PAW)[3] potential and the plane-wave basis with an energy cutoff of 500 eV. The exchange-correlation functional was treated using the Perdew-Burke-Ernzerhof(PBE)[4] generalized-gradient approximation(GGA)[4, 5]. For Brillouin-zone integrations, a Γ -centered dense mesh of 13×13×1 k points [6] is used for van der Waals heterostructures. The convergence criterion of the self-consistency process is set to be 10^{-5} eV.In our calculation, spin-orbit coupling (SOC) effects are taken into account and the interlayer van der Waals interaction is treated by DFT-D2 approximation [7].

The in-plane lattice parameters $a = b$ derived within the DFT approach are found to be 3.351 Å for $MoSe_2$ and 3.353 Å for WSe_2. The values fit experimental ones well and show very slight lattice mismatch between the two materials, which provides us a convenient method to construct AA stacking van der Waals heterostructures simply keeping the in-plane lattice parameters of single material unchanged. From Fig. S1. one can find out that, although the interlayer distances vary a little with the different in-plane lattice constants, the energy dispersions of the two van der Waals heterostructures under extreme conditions fit exactly. Since the real atomic configuration of the AA-stacking WSe_2/$MoSe_2$ van der Waals Heterostructures locates within the two extreme conditions, one can find out that our First-Principles band structures capture the characteristics of the reality.

Since the WSe_2/$MoSe_2$ van der Waals Heterostructures posses a Type-II heterostructures, we performed a series of First-principles calculations to investigate the validities of the monolayer Hamiltonians applied in the Letter. From Fig. S2, one can find out that, the band structures of the AA stacked WSe_2/$MoSe_2$ van der Waals Heterostructures can be treated as simple combinations of the individual monolayers. Neither the direct band gaps nor the band dispersions changed in the vicinity of the K or $K^{'}$ point in the Brillouin Zone, because of the interlayer interactions are much weaker than the intralayer bindings. Therefore, we can reach the conclusion that the monolayer Hamiltonians remain valid in our proposal.

S2. EXCITON HAMILTONIAN IN VAN DER WAALS HETEROSTRUCTURES

For specificity, we only discuss A-type bright excitons consisting of a spin-up electron in the bottom layer and a spin-down hole in the top layer. The Hamiltonian of a spin up electron in K valley is given by [8]

$$H_{\uparrow} = at(k_x\sigma_x + k_y\sigma_y) + \frac{\Delta - \lambda}{2}\sigma_z + \frac{\lambda}{2}. \tag{S1}$$

The total kinetic energy is $T_t = H_{1\uparrow} - H_{2\uparrow}$, where $H_{1\uparrow(2\uparrow)}$ denote spin up electron(spin down hole) Hamiltonian. In matrix form, the total Hamiltonian is

$$H_t = \begin{pmatrix} H_c & O \\ O^{\dagger} & H_v \end{pmatrix}, \tag{S2}$$

where

$$H_c = \begin{pmatrix} \epsilon_1 & -a_2t_2k_2^- \\ -a_2t_2k_2^+ & \epsilon_2 + V(\mathbf{r}_1 - \mathbf{r}_2) \end{pmatrix}, \qquad O = \begin{pmatrix} a_1t_1k^- & 0 \\ 0 & a_1t_1k^- \end{pmatrix},$$

and $H_v = \lambda_1 - \frac{\Delta_1+\lambda_2}{2} - \frac{\Delta_2-\lambda_2}{2}\sigma_z$, with non-diagonal terms neglected, as we only concern low momentum behavior. In the above expressions, $\epsilon_1 = (\Delta_1 - \Delta_2)/2$, $\epsilon_2 = (\Delta_1 + \Delta_2)/2 - \lambda_2$ and $V(\mathbf{r}_1 - \mathbf{r}_2)$ is the Coulomb potential between electrons and holes. The total wavefunction $\Psi = (\Psi_c, \Psi_v)^T$, where $\Psi_c = [\phi_{c1,c2}, \phi_{c1,v2}]^T$, $\Psi_v = [\phi_{v1,c2}, \phi_{v2,v2}]^T$. The total Hamiltonian contains the coupling between different components of the wave function Ψ. We can perturbatively eliminates other components of the wave function in favor of the exciton wave function $\phi_{c1,v2}$ that we are concerned [9].

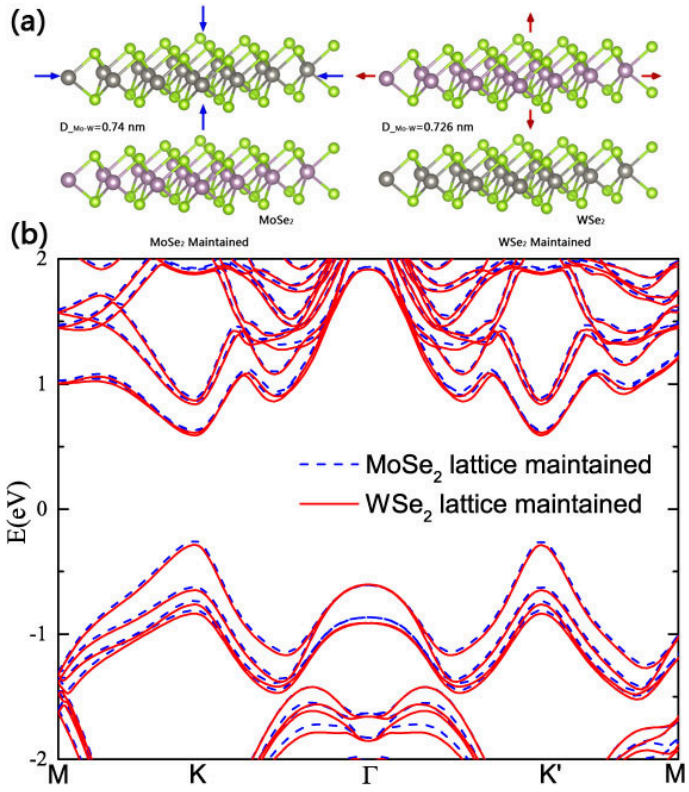

FIG. S1: (color online) (a) Schematic of the two extreme conditions of the AA-stacking $WSe_2/MoSe_2$ van der Waals Heterostructures. The pink and iron atoms indicate Mo and W respectively. As a consequece, maintaining the in-plane lattice constant of $MoSe_2$ will compress WSe_2 and maintaining the in-plane lattice constant of WSe_2 will strentch $MoSe_2$. (b) Band Structures of the two extreme cases. and the band structures fit well in vicinity of the Fermi surface (0 in the energy scale).

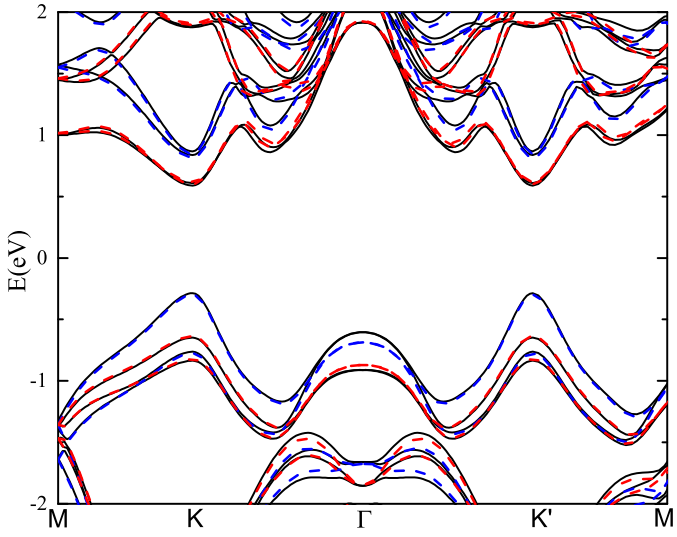

FIG. S2: (color online) Comparison of band structures between AA stacked $WSe_2/MoSe_2$ van der Waals Heterostructures and individual monolayer materials. The black solid lines indicate the band structure of AA stacked $WSe_2/MoSe_2$ van der Waals Heterostructure, the blue dashed lines indicate the band structure of individual WSe_2 monolayer while the red dashed lines indicate the band structure of individual $MoSe_2$ monolayer.

The eigenvalue problem can be expressed as

$$\begin{pmatrix} H_c & O \\ O^\dagger & H_v \end{pmatrix}\begin{pmatrix} \Psi_c \\ \Psi_v \end{pmatrix} = \epsilon\begin{pmatrix} \Psi_c \\ \Psi_v \end{pmatrix}. \tag{S3}$$

We can eliminate $\Psi_v = (\epsilon - H_v)^{-1}O^\dagger\Psi_c$ to obtain the equation $H_c^{\text{eff}}\Psi_c = \epsilon\Psi_c$ for Ψ_c, with

$$H_c^{\text{eff}} = H_c + O(\epsilon - H_v)^{-1}O^\dagger = \begin{pmatrix} \epsilon_1 & -a_2t_2k_2^- \\ -a_2t_2k_2^+ & \epsilon_2 + V(\mathbf{r}_1 - \mathbf{r}_2) + \frac{\hbar^2k_1^2}{2m_1} \end{pmatrix}. \tag{S4}$$

Then we further eliminate $\phi_{c1,c2}$ to obtain the exciton Hamiltonian acting on the exciton component $\phi_{c1,v2}$:

$$H_{ex} = \epsilon_2 + V(\mathbf{r}_1 - \mathbf{r}_2) + \frac{\hbar^2k_1^2}{2m_1} + \frac{\hbar^2k_2^2}{2m_2}. \tag{S5}$$

where the effective mass m_1 and m_2 are dependent on the eigenvalue ϵ:

$$m_1 = \frac{\hbar^2[\epsilon + (\Delta_1 - \Delta_2)/2 + \lambda_2 - \lambda_1]}{2a_1^2t_1^2}, \qquad m_2 = \frac{\hbar^2[\epsilon - (\Delta_1 - \Delta_2)/2]}{2a_2^2t_2^2}.$$

To get the internal energy levels of the exciton, we transform $(\mathbf{r}_1, \mathbf{r}_2)$ into the center-of-mass coordinate $\mathbf{R} = \alpha\mathbf{r}_1 + \beta\mathbf{r}_2$ and relative coordinate $\mathbf{r} = \mathbf{r}_1 - \mathbf{r}_2$, where

$$\alpha = \frac{m_1}{m_1 + m_2}, \quad \beta = \frac{m_2}{m_1 + m_2}. \tag{S6}$$

As the exciton Hamiltonian conserves the total momentum $\hat{\mathbf{P}} = \hat{\mathbf{p}}_1 + \hat{\mathbf{p}}_2$, the exciton Hamiltonian can be separated into the center-of-mass motion and the internal motion,

$$H_{ex} = \frac{\hat{\mathbf{P}}^2}{2M} - \frac{\hbar^2\nabla_{\mathbf{r}}^2}{2m_r} + V(\mathbf{r}) + \frac{\Delta_1 + \Delta_2}{2} - \lambda_2, \tag{S7}$$

where

$$M = m_1 + m_2, \quad m_r = \frac{m_1m_2}{m_1 + m_2}, \tag{S8}$$

The exciton eigenstate can be written as $\phi_{c1,v2} = e^{i\mathbf{P}\cdot\mathbf{R}/\hbar}\phi_{cv}(\mathbf{r})$, i.e., the product of the center-of-mass part $e^{i\mathbf{P}\cdot\mathbf{R}}$ and the internal part $\phi_{cv}(\mathbf{r})$. The exciton state excited by the light under consideration corresponds to vanishingly small momentum $\mathbf{P} \approx 0$. As we are interested in low-energy exciton states, we replace the exciton energy ϵ in $M(\epsilon)$ and $m_r(\epsilon)$ by the ground state energy $\epsilon_0 \approx 0.96$ eV. This gives the exciton mass $M(\epsilon_0) \simeq 0.64m_e$ (m_e the free electron mass).

S3. ORIGIN OF GAUGE POTENTIAL

In the CM coordinate representation, the total Hamiltonian $\hat{H}(\mathbf{R}, -i\nabla) = (-i\nabla)^2/(2M) + \hat{H}_{\text{in}}(\mathbf{R})$ is a 3×3 matrix in the internal state basis $|g\rangle, |1\rangle, |2\rangle$. The total state $|\Psi(\mathbf{R}, t)\rangle \equiv \langle\mathbf{R}|\Psi(t)\rangle$ is a 3×1 column vector describing the internal dynamics. The probability for the particle CM coordinate to be $\mathbf{R}$ is $\langle\Psi(\mathbf{R}, t)|\Psi(\mathbf{R}, t)\rangle$. Using the eigenstates $\{|\chi_i(\mathbf{R})\rangle\}$ with eigenvalues $\{\lambda_i(\mathbf{R})\}$ of $\hat{H}_{\text{int}}(\mathbf{R})$, $|\Psi(\mathbf{R}, t)\rangle$ is expanded as

$$|\Psi(\mathbf{R}, t)\rangle = \sum_i \Phi_i(\mathbf{R}, t)|\chi_i(\mathbf{R})\rangle,$$

where $|\Phi_i(\mathbf{R}, t)|^2 = |\langle\chi_i(\mathbf{R}), \mathbf{R}|\Psi(t)\rangle|^2$ is the probability for the particle to be in state $|\mathbf{R}\rangle|\chi_i(\mathbf{R})\rangle$, e.g., $\langle\Psi(\mathbf{R}, t)|\Psi(\mathbf{R}, t)\rangle = \sum_i |\Phi_i(\mathbf{R}, t)|^2$. From $\hat{H}(\mathbf{R}, -i\nabla_{\mathbf{R}})|\Psi(\mathbf{R}, t)\rangle = i\partial_t|\Psi(\mathbf{R}, t)\rangle$, we have

$$\mathbf{H}_{3\times3}(\mathbf{R})\begin{bmatrix}\Phi_1(\mathbf{R}, t)\\ \Phi_2(\mathbf{R}, t)\\ \Phi_3(\mathbf{R}, t)\end{bmatrix} = i\partial_t\begin{bmatrix}\Phi_1(\mathbf{R}, t)\\ \Phi_2(\mathbf{R}, t)\\ \Phi_3(\mathbf{R}, t)\end{bmatrix},$$

where the effective CM Hamiltonian

$$\begin{aligned}\mathbf{H}_{ij}(\mathbf{R}) &\equiv \delta_{ij}\lambda_i + \frac{1}{2M}\langle\chi_i|(-i\nabla)^2|\chi_j\rangle \\ &= \delta_{ij}\lambda_i + \frac{1}{2M}\sum_k [\delta_{ik}(-i\nabla) - \mathbf{A}_{ik}]\cdot\Big[\delta_{jk}(-i\nabla) - \mathbf{A}_{kj}\Big],\end{aligned}$$

where $\mathbf{A}_{ij}(\mathbf{R}) \equiv i\langle\chi_i|\nabla\chi_j\rangle = \mathbf{A}^*_{ji}(\mathbf{R})$. In matrix form, we have

$$\mathbf{H}_{3\times3}(\mathbf{R}) = \mathrm{diag}\{\lambda_1,\lambda_2,\lambda_3\} + \frac{1}{2M}\begin{bmatrix} -i\nabla - \mathbf{A}_{11} & -\mathbf{A}_{12} & -\mathbf{A}_{13} \\ -\mathbf{A}_{21} & -i\nabla - \mathbf{A}_{22} & -\mathbf{A}_{23} \\ -\mathbf{A}_{31} & -\mathbf{A}_{32} & -i\nabla - \mathbf{A}_{33}\end{bmatrix}^2.$$

In the Born-Oppenheimer approximation, the coupling between different components are neglected and we only keep the diagonal element

$$\begin{aligned}\mathbf{H}_{ii}(\mathbf{R}) &= \lambda_i + \frac{1}{2M}\Big[\mathbf{P}^2 - \mathbf{P}\cdot\mathbf{A}_{ii} - \mathbf{A}_{ii}\cdot\mathbf{P}\Big] + \frac{1}{2m_0}\sum_k \mathbf{A}_{ik}\cdot\mathbf{A}_{ki} \\ &= \lambda_i + \frac{1}{2M}\Big[\mathbf{P}^2 - \mathbf{P}\cdot\mathbf{A}_{ii} - \mathbf{A}_{ii}\cdot\mathbf{P}\Big] + \frac{1}{2m_0}\langle\nabla\chi_i|\cdot|\nabla\chi_i\rangle \\ &= \lambda_i + \frac{1}{2M}(\mathbf{P} - \mathbf{A}_{ii})^2 + \frac{1}{2m_0}\Big(\langle\nabla\chi_i|\cdot|\nabla\chi_i\rangle - |\langle\chi_i|\nabla\chi_i\rangle|^2\Big).\end{aligned}$$

* Corresponding Author: kchang@semi.ac.cn

[1] P. Hohenberg and W. Kohn, Phys. Rev. B **136**, 864 (1964).
[2] G. Kresse and J. Furthmuller, Phys. Rev. B **54**, 11169 (1996).
[3] G. Kresse and D. Joubert, Phys. Rev. B **59**, 1758 (1999).
[4] J. P. Perdew, K. Burke and M. Ernzerhof, Phys. Rev. Lett. **77**, 3865 (1996).
[5] J. P. Perdew and Y. Wang, Phys. Rev. B **33**, 8800 (1986).
[6] H. J. Monkhorst and J. D. Pack, Phys. Rev. B **13** 5188 (1976).
[7] S. Grimme, J. Comp. Chem. **27**, 1787 (2006).
[8] D. Xiao, G. B. Liu, W. X. Feng, *et al.*, Phys. Rev. Lett. **108**, 196802 (2012).
[9] P. O. Löwdin, J. Chem. Phys. **19**, 1396 (1951).